A new catechol-functionalized polyamidoamine as an effective SPION stabilizer

Galli, Marco; Rossotti, Beatrice; Arosio, Paolo; Ferretti, Anna Maria; Panigati, Monica; Ranucci, Elisabetta; Ferruti, Paolo; Salvati, Anna; Maggioni, Daniela

Published in:
Colloids and Surfaces B: Biointerfaces

DOI:
10.1016/j.colsurfb.2018.11.007

Publication date:
2019

Colloids and Surfaces B: Biointerfaces 174 (2019) 260–269

Contents lists available at ScienceDirect

Colloids and Surfaces B: Biointerfaces

journal homepage: www.elsevier.com/locate/colsurfb

Protocols

A new catechol-functionalized polyamidoamine as an effective SPION stabilizer

Marco Galli[a], Beatrice Rossotti[a], Paolo Arosio[b,e], Anna Maria Ferretti[c], Monica Panigati[a,f], Elisabetta Ranucci[a,e], Paolo Ferruti[a,e], Anna Salvati[d], Daniela Maggioni[a,e,*]

[a] Dipartimento di Chimica, Università degli Studi di Milano, Via Golgi 19, 20133 Milano, Italy
[b] Dipartimento di Fisica, Università degli Studi di Milano, Via Celoria 16, 20133 Milano, Italy
[c] Laboratorio di Nanotecnologie, CNR-Istituto di Scienze e Tecnologie Molecolari, Via G. Fantoli 16/15 I, 20138 Milano, Italy
[d] Groningen Research Institute of Pharmacy, University of Groningen, A. Deusinglaan 1, 9713 AV Groningen, the Netherlands
[e] Consorzio INSTM, via G. Giusti 9, 50121, Firenze, Italy
[f] Istituto per lo studio delle macromolecole, Consiglio Nazionale delle Ricerche (ISMAC-CNR), Via A. Corti 12, 20133 Milano, Italy

ARTICLE INFO

Keywords:
SPION
Polyamidoamine
Ligand exchange
Relaxivity

ABSTRACT

A synthetic strategy was established for decorating and stabilizing superparamagnetic iron oxide nanoparticles (SPIONs) with a zwitterionic linear polyamidoamine (PAA). The strategy was successfully tested with a PAA coded ISA23 previously found endowed with interesting biological properties, such as biocompatibility, degradability in aqueous media and stealth-like properties when injected in test animals. A post-synthetic functionalization with catechol-bearing moieties of a preformed PAA was successfully carried out. ISA23 was obtained by polyaddition reactions of methyl-piperazine and 2,2-bis(acrylamidoacetic) acid. It was functionalized using nitrodopamine and 1-ethyl-3-(3-dimethylaminopropyl)carbodiimide as coupling agent, to randomly form amide bonds with 17% of ISA23 carboxylic groups (ISA23-ND). SPIONs were prepared by a thermal decomposition synthesis in 1-octadecene with oleic acid, and then transferred in water by two distinct ligand exchange procedures: i) the direct displacement of oleate molecules from SPION surface by ISA23 in a biphasic (n-hexane/water) environment; ii) the two-step method involving an intermediate small molecule, tetramethylammonium hydroxide, used as a transient transfer agent, which was in turn exchanged with ISA23-ND in a second exchange step occurring in water. The two-step procedure provided a SPION@PAA nanocomposite more stable than that obtained by the one-step procedure in the presence of an applied external magnetic field. ATR-FTIR spectroscopy, ζ-potential and thermogravimetric analysis (TGA) showed the presence of the ISA23 on the SPION surface. In particular, TGA showed that the ISA23-ND amount on the NPs accounted for 26% of the overall nanocomposite mass. The nanocomposite size was determined by both TEM (21.1 ± 2.9 nm) and DLS measurements (hydrodynamic size 100 ± 28 nm). SPION@ISA23-ND were re-suspended after lyophilization reverting to their pristine dimensions. The SPION@ISA23-ND adsorption of BSA in water, considered as the first stage of phagocytosis, was very low, suggesting that ISA23 could impart stealthiness to SPION@ISA23-ND.

^{1}H-NMR relaxivity measurements showed an r_2 value of 158 s^{-1} $mmol^{-1}$ L (vs 100 s^{-1} $mmol^{-1}$L for Endorem®) at relevant clinical fields for magnetic resonance imaging (from 0.2 to 1.5 T). SPION@ISA23-ND was tested on HeLa cells and their internalization was visualized by reflectance microscopy.

Finally, with the aim of prepare a new dual magneto-optical system, a synthetic procedure to decorate SPION@ISA23-ND with a fluorescent dye was devised, even though the emission intensity of the resultant conjugate was lower than expected, possibly due to luminescence quenching caused by the closeness of emitting moieties to the SPION surface.

1. Introduction

Superparamagnetic iron oxide nanoparticles (SPIONs) have long since been in the spotlight as promising candidates for a plethora of biomedical applications [1], including magnetic resonance imaging (MRI) [2], magnetic particle imaging (MPI) [3,4], and magnetofluidic hyperthermia (MFH) [5,6], thanks to their peculiar magnetic properties and high biocompatibility. The thermal decomposition of

* Corresponding author at: Dipartimento di Chimica, Università degli Studi di Milano, Via Golgi 19, 20133 Milano, Italy.
E-mail address: daniela.maggioni@unimi.it (D. Maggioni).

https://doi.org/10.1016/j.colsurfb.2018.11.007
Received 9 July 2018; Received in revised form 17 October 2018; Accepted 3 November 2018
Available online 12 November 2018

organometallic precursors in high-boiling organic solvents in the presence of surfactants such as oleic acid represents the best method to produce SPIONs with high magnetic properties [7,8]. However, the resultant SPIONs are dispersible only in apolar organic solvents. In order to render them dispersible in water, hence suitable for in vivo uses, a hydrophilic stabilizing coating capable to prevent aggregation and sedimentation by either repulsion or steric hindrance is needed [9,10]. Once injected in the bloodstream, the coating should also prevent SPION opsonization and recognition by the reticulo-endothelial system (RES), thus prolonging their circulation time and maximizing their chances to reaching the target tumour and concentrate there thanks to the so-called “enhanced permeability and retention” (EPR) effect [11].

One of the most widely adopted approaches to transfer NPs stabilized with hydrophobic coatings from organic to aqueous phases is the use of small amphiphilic organic molecules containing both a functional group with affinity for the NP surface and a second functional group with water affinity [12,13]. Amphiphilic polymers capable to form by intercalation stable weak interactions with the hydrophobic layer on NP surface and to expose to the environment the hydrophilic residues are also used [14,15]. Alternatively, organic or inorganic polymers as for instance dextran [16], silica [17–20] or PEG [21–23] have been employed as biocompatible cover for magnetic nanoparticles obtained in many cases by coprecipitation methods. Not surprisingly, owing to the scientific and clinical relevance of superparamagnetic iron oxide nanoparticles in ferrofluids, a large patent literature on their stabilizing and biocompatibilizing covers exists [24–29].

In this work, a new polymeric SPION stabilizing coating was developed, based on an amphoteric polyamidoamine (PAA) coded ISA23, bearing both one carboxyl and two *tert*-amine groups per repeating unit (Scheme 1). ISA23 is highly hydro-soluble and was previously found to be biocompatible, biodegradable, and to exhibit “stealth-like” properties once injected in animals [30–32].

Therefore, it could be expected that this polymer, properly functionalized to make it adhesive to SPION surface, was able to render them hardly recognized by the reticuloendothelial system (RES).

ISA23, as all PAAs, is characterized by high structural versatility, being easily modified by copolymerization techniques, since the Michael addition reaction between prim- or sec-amines and bisacrylamides is specific and many different functions do not interfere and can be introduced as side substituents [33–36].

Thanks to the exceptional iron affinity of catechol, exploited by a variety of natural siderophore proteins [37], many examples of polymers bearing multiple catechol pendants were proposed for tightly binding NPs and stabilizing their colloidal dispersions [38,39].

The first step of the synthetic strategy adoptedwas to introduce in ISA23 catechol pendants capable of giving stable bonds with the surface of iron oxide. The procedure consisted of conjugating a part of its carboxyl groups with nitrodopamine by means of 1-ethyl-3-(3-dimethylaminopropyl)carbodiimide (EDC) as coupling agent. The new SPION-ISA23 composites were fully characterized and their response to external magnetic fields of clinical relevance for magnetic resonance imaging discussed. A synthetic pathway to decorate with fluorescent probes SPION-ISA23 nanocomposites and obtain magneto-optical NPs for easier monitoring internalization in vitro [40] was also devised.

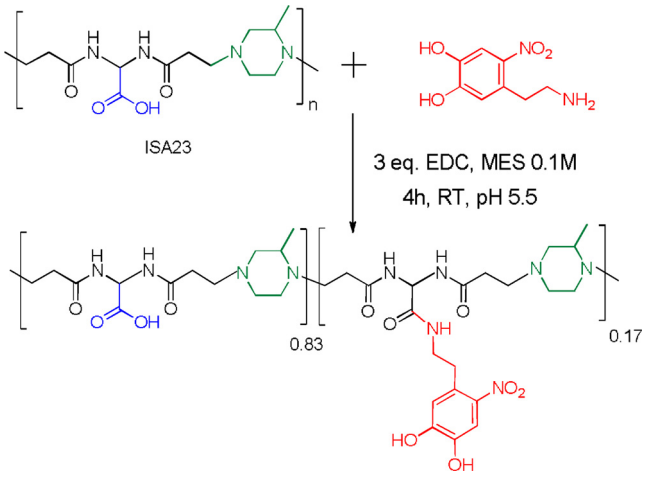

Scheme 1. Synthesis of ISA23-ND.

2. Results and discussion

2.1. Synthesis of ISA23-nitrodopamine copolymer conjugate

The synthesis of ISA23 is reported elsewhere [30]. It was based on the Michael-type polyaddition of 2-methylpiperazine with 2,2-bis(acrylamido acetic) acid (Scheme S1). The ISA23-nitrodopamine conjugate (henceforth called ISA23-ND) was obtained by reacting part of ISA23 side carboxyl groups with the amine group of 2-nitrodopamine using 1-ethyl-3-(3-dimethylaminopropyl)carbodiimide (EDC) as coupling agent in a pH 5.5 2-(N-morpholino)ethanesulfonic acid (MES) buffer solution (Scheme 1). Nitrodopamine was preferred to dopamine owing to its stronger binding affinity and its higher stability towards oxygen- and metal-catalysed self-oxidation [6].

ISA23-ND was purified by ultrafiltration through centrifugation (3000 Da cut-off filter). The retained portion was freeze-dried giving the product as a fluffy yellow solid. In order to maintain the amphoteric nature of parent ISA23, 17% of its carboxylic groups, as determined by the integrated intensities of the ^{1}H-NMR signals of the H atom α to the newly formed amide groups and of those of the H atom α to the unmodified ISA23 carboxyl group (Fig. S1), were employed in the coupling reaction.

ISA23-ND showed the typical UV–vis pH dependant absorption bands of nitrocatechols arising from different protonation states of the catechol group [41] (Fig. 1a). At acidic pH the main peak was observed at 305 nm, which at higher pH shifted to 398 nm (with a minor absorption at ~280 nm) due to deprotonation of one hydroxyl group of catechol. After 24 h, at pH 12.5 two maxima in the absorption profile (409 and 500 nm), corresponding to the deprotonation of both the catechol hydroxyl groups were observed (blue trace in Fig. 1a).

The thermogravimetric analysis (TGA) of ISA23-ND in air showed different weight loss steps, with complete degradation at ~600 °C (see Fig. 1b), similarly to what previously observed for ISA23 [42]. The first step (50–170 °C, ~15%) was ascribed to the release of hydration water. The second step (T onset 210 °C, ~60% ca) is tentatively attributed to the release of volatile 2-methylpiperazine. Indeed, it is known that PAAs decompose at high temperatures by retro-Michael reactions giving off the starting amines and bisacrylamides [43]. Finally, the residue completely volatilized by oxidation (T onset 460 °C, ~25%).

It is well known that linear PAAs are able to self-assemble in aqueous solution producing spherical nanoparticles [33,34]. The DLS size distribution of ISA23-ND showed a main population formed by nanoaggregates with diameter smaller than 10 nm, with larger aggregates (intensities distribution Fig. S2 top), accounting only for a negligible fraction of the material, as indicated by the volume distribution (Fig. S2 bottom).

The pH dependence of the ζ-potential (Fig. 1c) accounts for the amphoteric nature of ISA23, the contribution of the small fraction of nitrodopamine moieties in ISA23-ND being negligible in this respect, and well agrees with its ionic species distribution (Fig. 1d): positive charge at acidic pH, zero charge point at pH close to the isoelectric point (ISA23 IP = 5.5) due to zwitterion formation, and negative charge at basic pH, where both carboxyl and amino groups are deprotonated.

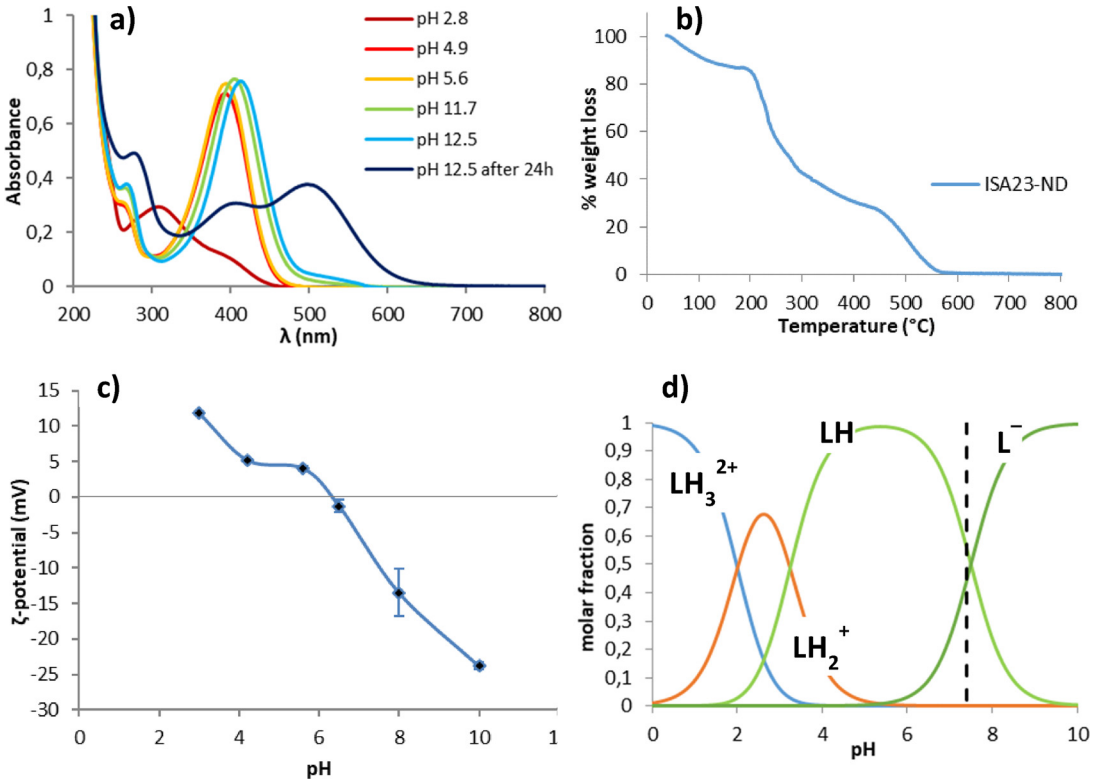

Fig. 1. Characterization of ISA23-ND. a) pH dependent UV–vis absorption spectra in aqueous solution; b) TG thermogram; c) ζ-potential curve; d) ISA23 speciation curves versus pH. The dashed vertical line indicates pH 7.4 (For interpretation of the references to colour in this figure legend, the reader is referred to the web version of this article).

2.2. Synthesis of iron oxide @ ISA23-ND nanocomposite

Iron oxide NPs were prepared by thermal decomposition of iron pentacarbonyl in refluxing 1-octadecene, using a slightly modified literature procedure [44] (see Experimental part for details), providing oleate-capped NPs easily dispersible in n-hexane. DLS analysis (Fig. S3) showed that the synthesized SPIONs were monodisperse, with slightly different sizes (mean hydrodynamic diameter 26.6 ± 3 nm and 30.8 ± 4.8 nm) by introducing small variations in the experimental conditions (Fe:OA ratio and absolute concentration).

Two different methods were investigated for transforming the oleate-coated SPIONs into the target SPION@ISA23-ND nanocomposites.

2.3. Direct one-step ligand exchange

Due to the insolubility of ISA23-ND in solvents other than water, literature methods that use polar organic solvent mixtures, such as THF – ethanol [45], for exchanging the capping ligand on the NPs could not be adopted. As an alternative approach, a direct exchange from hexane to water was first investigated. Ultrasonication was used to create an oil-in-water emulsion between the hexane dispersion of the oleate-coated NPs and the aqueous ISA23-ND solution, similarly to a literature procedure employing a catechol functionalized chitosan [46]. The effective ligand exchange (Scheme S2) was achieved only after the pH was adjusted at acidic values (pH ~3–4), to protonate the leaving oleate molecules, thus increasing their affinity for the organic phase [47].

TEM analysis (Fig. S4) showed that the SPION@ISA23-ND nanocomposites prepared in this way were of regular shape and monodisperse, with a core diameter of 15.8 ± 1.7 nm (dispersion 10.7%). A polymer coating shell of ~2 nm thickness was clearly visible around each NP. The occurrence of the ligand exchange was further evidenced by the ζ-potential curve (Fig. 2a), which showed a pH dependence similar to that of the parent ISA23-ND (Fig. 1c). Not unexpectedly, the mean NP size measured by TEM was smaller than that of the native SPION@OA provided by DLS (26–30 nm, see above), since the latter technique measures the hydrodynamic diameter that includes the solvent corona moving consistently to the NP.

DLS analysis of SPION@ISA23-ND showed a single broad peak corresponding to a mean hydrodynamic diameter of ~180 nm (Fig. 2b), consistent with the presence of large aggregates. The tendency of ISA23 derivatives to form aggregates with iron oxide NPs was previously reported [48], even if the preparation procedure was different (coprecipitation method in the presence of the PAA). It was speculated that during the exchange of oleic acid and ISA23-ND at NP surface, while oleic acid detaches, NPs concentrate at the interphase between the two non-mixable solvents where they can partly aggregate prior to polymer binding to the NP surface. This hypothesis was supported by the evidence that NPs were mostly found in the interphase layer between hexane and water.

The TG profile of SPION@ISA23-ND (Fig. 2c, blue line) showed an initial weight loss due to hydration water (~3%), and that the weight loss due to the thermo-oxidative decomposition of organic layer (onset temperature of 210 °C) accounted for about the 11% of the total nanocomposite weight.

Cellular internalization studies were carried out in HeLa cells exposed for 24 h to 30 μg/mL NPs. No obvious sign of toxicity was detected, and cell density and phenotype were comparable to control untreated cells. Being NPs not fluorescent, reflected light microscopy [49–52] was used (Fig. 2d). This imaging technique does not allow distinguishing single NPs, but has the merit of not requiring labelling. Moreover, it allows establishing correlation with confocal microscopy to confirm the particle location, especially in the case of multiple particles trafficking together into specific cell compartments.

The lysosomes were visualized by immuno-staining the lysosomal

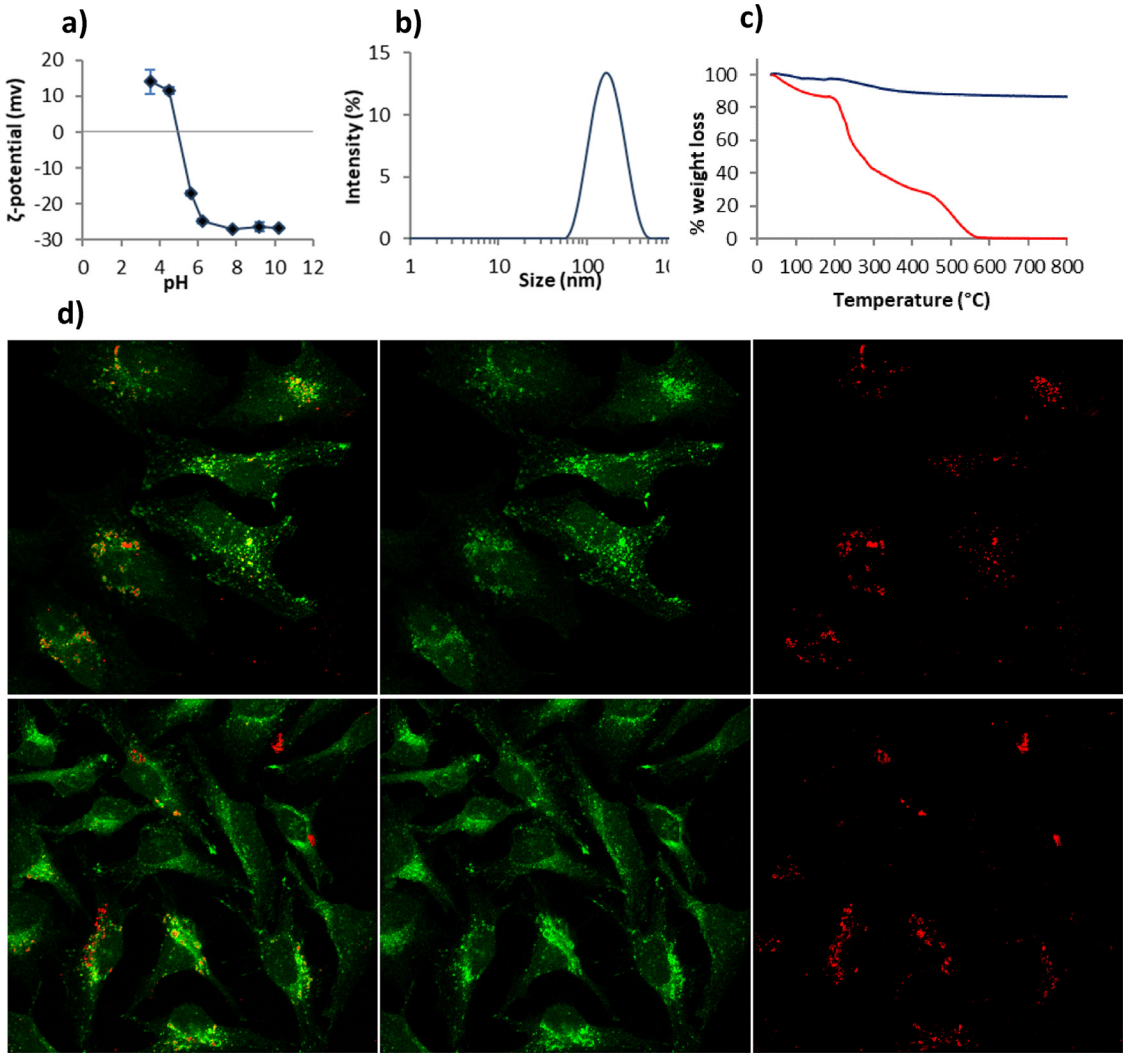

Fig. 2. Characterization of SPION@ISA23-ND. a) ζ-potential curve; b) DLS intensity size distribution; c) TG thermogram for SPION@ISA23-ND (blue trace) compared to the curve for ISA23-ND (red trace) of Fig. 1b; d) Reflected light microscopy of SPION@ISA23-ND. HeLa cells were exposed to 30 μg/mL of NPs for 24 h. LAMP-1 staining with Alexa 488 was used to visualize the lysosomes in the cells (in green). Two distinct zoom-in snapshots are presented on the two lines. Left: superposition of reflected light (red) and lysosome fluorescence (green); center: lysosome fluorescence only of the same snapshot; right: reflected light only (For interpretation of the references to colour in this figure legend, the reader is referred to the web version of this article).

protein LAMP-1 (green staining). From these images it can be concluded that the NPs were indeed internalized by the cells. As expected and commonly observed for most nanomaterials, the NPs were mainly present at lysosome level, as a consequence of a probable endocytic mechanism of internalization [53].

The NPs synthesized by this method showed heavy aggregation when placed under an external magnetic field, hampering relaxometric characterization. In order to avoid this detrimental effect an alternative procedure was developed.

2.4. Two-step ligand exchange

The two-step procedure involved the treatment of the hydrophobic oleate-stabilized NPs with an intermediate water-transferring agent, to be subsequently replaced by ISA23-ND. In this work, tetramethylamonium hydroxide (TMAOH) was used as water-transfer agent, a non-coordinating species commonly used as transfer agent for magnetite NPs [54–56].

According to the adopted procedure, dried SPION@OA were dispersed in a 0.125 M aqueous TMAOH solution, giving rise to a stable water suspension of SPION@TMAOH nanoparticles (first part of Scheme S3). The number size distribution from DLS measurements (Fig. S5 bottom) showed that the large majority of the NPs had a mean hydrodynamic diameter equal to 40 ± 9 nm (from intensities graph, Fig. S5 top). After washing twice by centrifugation to remove any TMAOH excess, SPION@TMAOH were treated with a threefold amount in weight of ISA23-ND, under shaking at room temperature for 72 h (Scheme S3). The so obtained SPION@ISA23-ND nanoparticles showed, after purification, an increase in hydrodynamic diameter, peaking at 100 nm, by Intensities distribution (Fig. 3a). It is worth noting that, differently from the direct ligand exchange procedure, the OA/TMAOH exchange proceeded very fast (5 min duration) preventing the early SPION aggregation. Moreover, since the TMAOH/ISA23-ND exchange to give SPION@ISA23-ND occurred in a homogeneous aqueous phase, there were no favourable conditions for NP aggregation (see above direct ligand exchange procedure).

The presence of the ISA23-ND on SPION surface was proved by several pieces of evidence. Attenuated total reflection-Fourier transform infrared spectroscopy (ATR-FTIR) showed that the TMAOH/ISA23-ND exchange had actually occurred. Indeed, the two sharp and strong bands at 1488 cm^{-1} and 950 cm^{-1}, characteristic of TMAOH (CH_3 asymmetric deformation mode and of the C–N asymmetric stretching

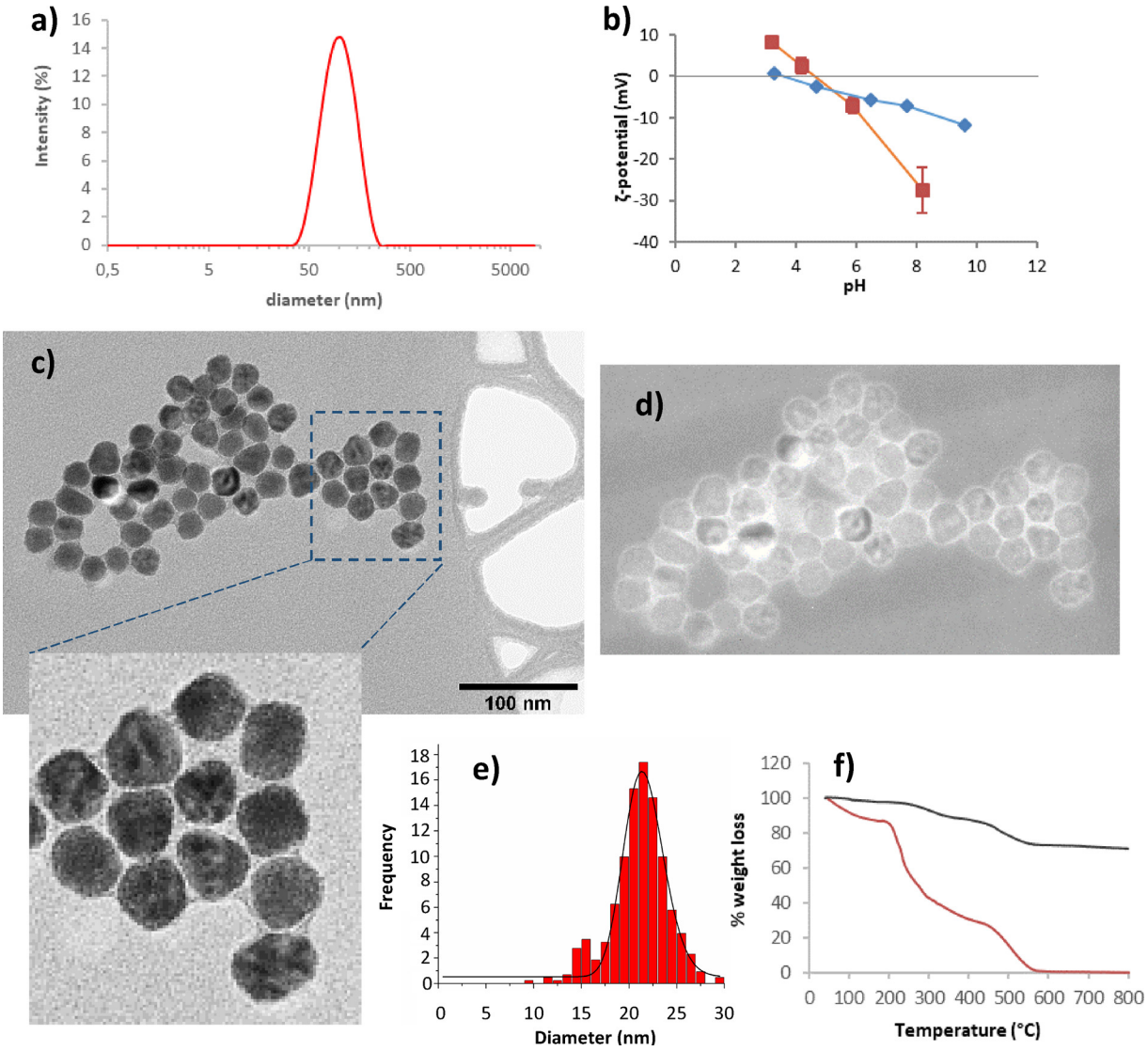

Fig. 3. Characterization of the SPION@ISA23-ND obtained by the two step procedure. a) DLS intensity distribution. b) ζ-potential of SPION@TMAOH (blue) and SPION@ISA23-ND (red); c) TEM image with a zoom-in region; d) Energy Selected TEM image collected at 24 eV ± 2 eV corresponding to the conventional TEM image reported in c; e) TEM size distribution of the inorganic core; f) comparison between the TG profiles of ISA23-ND (orange) and SPION@ISA23-ND obtained by the two step procedure (For interpretation of the references to colour in this figure legend, the reader is referred to the web version of this article).

[57], Fig. S6 middle) were no more visible in the SPION@ISA23-ND spectrum (Fig. S6 bottom). The latter spectrum showed both the typical bands of polyamidoamine and the intense vibrational band due to iron oxide core, centred at 573 cm^{-1} (Fe–O–Fe stretching modes of the spinel structure of magnetite) [58].

The comparison of the ζ-potential curves of SPION@TMAOH and SPION@ISA23-ND (Fig. 3b) in the pH range 3–10 further confirmed the occurrence of the ligand exchange. Particularly significant was the positive values at low pH shown by the PAA stabilized NPs that became strongly negative at higher pH values, according to the typical behaviour of amphoteric PAAs (see above).

TEM analysis (Fig. 3c–e) showed NPs with a core size equal to 21.1 ± 2.9 nm (dispersion 13.7%). The presence of polymer coating of irregular thickness was better highlighted by means of energy-selected imaging operating at 24 eV, which corresponds to the carbon component of the plasmon signal. The contrast-enhanced Fig. 3d shows the polymer shell surrounding each NP as a white halo around the dark iron oxide core.

The TG thermograms of SPION@ISA23-ND and ISA23-ND (Fig. 3f) showed that NPs underwent a total weight loss of 26% at temperatures corresponding to the volatilization of ISA23ND (from 200 to 600 °C). The weight loss was significantly higher than that observed for the nanocomposite obtained with the direct ligand exchange method (11%, blue trace in Fig. 2c). The thicker PAA coating was likely responsible for the observed nanocomposite stability in the magnetic field (see further).

Moreover, SPION@ISA23-ND could be re-suspended after lyophilization and reverted to their pristine dimensions without sonication.

The observed ISA23 stealthiness in the bloodstream [30] suggested that this property could be shared by SPION@ISA23-ND. Phagocytosis is triggered by plasma protein adsorption [59]. Reduced protein adsorption is considered an indication of plasma stability [60]. The adsorption of BSA (Bovine serum albumin) as a representative model serum protein may be considered as an indicator of the non-specific plasma protein adsorption [61–63]. SPION@ISA23-ND and SPION@TMAOH were incubated 90 min at room temperature with a BSA solution in phosphate buffer pH 7.4. UV–vis spectroscopy was used to determine the residual BSA in the supernatant (Fig. S7). SPION@TMAOH adsorbed a substantial BSA amount (23% of the original), whereas the BSA adsorption by SPION@ISA23-ND was negligible (~3% of the

original), clearly suggesting that ISA23-ND coating could endow NPs with stealth-like properties.

2.5. Synthesis of fluorescent SPION@PAA nanocomposites

With the aim of obtaining a dual magneto-optical system, a procedure was devised to decorate SPION@PAA core/shell NPs with a fluorescent dye. The first step was to design a nitrodopamine-bearing PAA functionalized with the fluorescent dye RhodamineB (RhodB from now on). A PAA bearing a thiol group in 10% of its repeating units ($ISA23SH_{10\%}$ in Scheme S4 top) was first reacted with nitrodopamine, following the same procedure described above for ISA23, resulting in functionalization of ~10% of the free carboxyl groups (Scheme S4). In a second step, Michael addition of the ISA23SH thiol groups with the ethylmaleimido group of the functionalized-RhodB [58] produced ISA23SH-ND-RhodB polymer (Scheme S4 bottom), whose UV–vis spectrum is reported in Fig. S8b. At 530 and 562 nm the typical peaks due to RhodB fragment were observed, while the bands due to the nitrodopamine pendent lie between 340 and 460 nm.

ISA23SH-ND-RhodB underwent the above described two-step ligand exchange procedure, involving the intermediate formation of SPION@TMAOH. The excess of polymer was removed via magnetic recovery of the nanocomposite and subsequent discard of the supernatant, obtaining water-dispersed SPION@ISA23SH-ND-RhodB nanoparticles, with a hydrodynamic diameter of ca 80 nm (Fig. S8a), and whose TEM image is reported in Fig. S9.

UV-vis spectroscopy of the purified particles showed superposition of the RhodB absorption band (λ_{max} = 559 nm) to the broad band of iron oxide NPs (Fig. S8a, red trace). The absorption bands of the nitrodopamine moiety were not visible since superimposed with the strong magnetite core absorption. The UV–vis spectrum of the supernatant after a centrifugation cycle (Fig. S8b, black trace) did not show any RhodB signal, proving that the RhodB functionalized polymer was actually bound to the SPION surface. Photoluminescence spectra were recorded for both SPION@ISA23SH-ND-RhodB and the free polymer. The emission spectra of the two compounds are almost superimposable, presenting the typical emission profile of RhodB with a maximum at 580 nm (Fig. S10). This proved that the emission energy of RhodB did not significantly change after conjugation to SPION (580 vs. 583 nm). However, the quantum yields dropped of about one order magnitude (0.3% vs. 2.5%, respectively), as already observed in other magneto-fluorescent nanosystems [64], and this prevented to exploit this nanocomposite as luminescent probe for monitoring its cell uptake by confocal microscopy or flow cytometry. It was speculated that this was due to the random closeness of RhodB units to the SPION surface.

2.6. Relaxometric characterization of two-step synthesized-SPION@ISA23-ND

In the framework of biomedical applications, the measurements of the nuclear relaxivities, i.e. the efficiency in contrasting the magnetic resonance images (MRI), are suitable to predict the efficiency of magnetic nanoparticles as contrast agents for MRI [65]. The nuclear relaxivities r_1 and r_2 are defined as:

$$r_i = \frac{1/T_{i,\,NP+water} - 1/T_{i,\,water}}{c}$$

where T_1 and T_2 represent the longitudinal and transverse nuclear relaxation times in presence (NP + water) or absence (water) of magnetic nanoparticles and c is the iron concentration of the sample.

In order to evaluate the ability of -SPION@ISA23-ND obtained by the two-step procedure to affect water nuclear relaxation times, ^{1}H-NMR relaxivity measurements were performed at magnetic fields relevant for MRI tomographs (H = 0.2, 0.5 and 1.5 T).

At these fields, the ^{1}H-NMR longitudinal nuclear relaxivity, $r_{1,}$ values of SPION@ISA23-ND (Table S1) were comparable to those of the commercial product. However, at the same clinical fields, the ^{1}H-NMR transverse nuclear relaxivity, r_2, values of SPION@ISA23-ND (Table S1) showed a 50% increase in r_2 values compared to Endorem®, the withdrawn commercial T_2 contrast agent still normally used for comparison in literature. Therefore, the r_2 values obtained for SPION@ISA23-ND lets envisage a potential as T_2 contrast agents in T_2 imaging [66]. Moreover, the higher r_2 values obtained in our system with respect to Endorem allow to conclude that, with the same amount of contrast agent, the contrast-to-noise-ratio in magnetic resonance images might reduce the injected doses.

3. Conclusions

A convenient strategy for decorating and stabilizing superparamagnetic iron oxide nanoparticles (SPIONs) with a zwitterionic biocompatible, degradable and stealth-like linear polyamidoamine was established. This procedure will be most likely employable for introducing catechol pendants on PAAs other than ISA23. This system exploited the well-known anchoring ability of catechol group to iron oxide and proved able to successfully stabilize SPIONs even for low amounts of catechol groups, to avoid detrimental effects on the polymer properties that might result from excessive functionalization. Owing to the versatility of PAAs as a polymer class, this opens the way to decorate SPIONs or other metal oxide nanoparticles with differently functionalized coatings.

Relaxometric characterization of SPION@ISA23-ND nanocomposite showed that they hold promising NMR efficiency when dispersed in water.

The hydrodynamic diameter of the SPION@ISA23-ND obtained in this way was smaller than 100 nm, sufficiently small size for in vivo applications, since the reticulo-endothelial system is less prone to recognizes and eliminate small NPs, especially if coated with zwitterionic coatings at physiological pH.

SPION@ISA23-ND could be re-suspended after lyophilization and reverted to their pristine dimensions without sonication. Moreover, the SPION@ISA23-ND adsorption of BSA in water, considered as the first stage of phagocytosis, was only ~3%, compared with 23% for SPION@TMAOH, suggesting that ISA23 coating could impart stealth-like behavior in the bloodstream.

Preliminary in vitro assays showed that SPION@ISA23-ND nanocomposite was well tolerated by Hela cells, where they localize inside lysosomes, as revealed by reflected light microscopy, exploiting their high scattering ability.

Finally, a successful synthetic procedure was devised to obtain dual magneto-optical probes, conjugating a novel PAA bearing both catechol and Rhodamine B pendants to the SPION surface. Low emission intensity was detected due to the luminescence quenching. Since this problem was likely due to the closeness of the RhodamineB to the SPION surface, it could be overcome by spacing the SPION surface and the dye moieties, through the introduction of new linkers.

4. Experimental part

4.1. Chemical and biological materials

All chemicals were purchased from Sigma Aldrich (including iron(0) pentacarbonyl) and used as received, if not otherwise specified.

Ultrapure water (milli-Q, Millipore, resistivity = 18 M Ω cm^{-2}) was used for the preparation of the aqueous solutions.

Human cervical cancer epithelial HeLa cells (from human cervix adenocarcinoma) were purchased from the American Type Culture Collection (ATCC − CCL2).

Minimal Essential Medium (MEM), Dulbecco modified Phosphate Buffer Saline (DPBS), Trypsin solution (porcine trypsin-EDTA 0.05%) and Fetal Bovine Serum (FBS) were purchased from Gibco, Thermo

Fisher Scientific. Complete medium (CMEM) was obtained by supplementing MEM with 10% FBS not heat inactivated (50 ml FBS added to 500 mL MEM).

Bovine serum albumin (50 kDa) was purchased from Sigma Aldrich.

4.2. Instruments

NMR experiments were performed on a Bruker DRX400 spectrometer equipped with a Bruker 5 mm BBI Z-gradient probe head with a maximum gradient strength of 53.5 G/cm in D_2O.

DLS and ζ-potential measurements were performed using a Malvern Zetasizer nano ZS instrument at 25 °C, equipped with a 633 nm solid state He–Ne laser at a scattering angle of 173°, typically dissolving samples at concentration 1 mg/mL or less. The size and charge measurements were averaged from at least three repeated measurements.

UV − vis absorption spectra were acquired on an Agilent model 8543 spectrophotometer at room temperature and using standard quartz cells with 1.0 cm path length.

Emission spectra were obtained with an Edinburgh FLS980 spectrofluorimeter equipped with a 450 W xenon arc lamp. Emission spectra were corrected for source intensity (lamp and grating) and emission spectral response (detector and grating) by standard correction curves. Photoluminescence quantum yields were measured with a Hamamatsu Photonics absolute PL quantum yield measurement system (C11347-01 Quantaurus spectrometer) equipped with a L11562 Xenon light source (150 W), monochromator, C7473 photonic multi-channel analyzer, integrating sphere and employing U6039-05 PLQY measurement software (Hamamatsu Photonics, Ltd., Shizuoka, Japan).

Thermogravimetric analysis. Thermogravimetric analysis (TGA) were performed in air in the temperature range 50–800 °C with a heating rate of 5 °C min^{-1}, using a Mettler-Toledo thermogravimetric balance (TGA/DSC 2 Star® System) on ca 5 mg of lyophilized samples.

ATR-FTIR spectroscopy. IR spectra were acquired on a PerkinElmer Frontier equipped with an ATR accessory with a diamond/ZnSe crystal.

Relaxometric characterization. The MRI contrast efficiency was assessed by means of ^1H nuclear magnetic resonance (NMR) relaxometric characterization. The NMR measurements were performed at room temperature by measuring the longitudinal and the transverse nuclear relaxation times T_1 and T_2 at the frequencies $\nu = 8.5$, 21.3 and 63.8 MHz. The NMR signal detection and generation was obtained by Stelar Spinmaster Fourier transform-nuclear magnetic resonance (FT-NMR) spectrometer.

Metal content on SPION was determined by a spectrophotometric method, digesting few microliters of nanoparticles suspension with 1 mL of concentrated HCL (37%) at RT for 1 night, directly in a 10 mL volumetric flask. Then, it was filled up with 100 u L of 10% w/w NH_2OH, acetate buffer solution (pH 4.6, 0.15 M, 6 mL), 1,10-phenantroline solution (0.6% w/w, H_2O/MeOH 10 : 1, 0.2 mL), and finally brought to volume with milliQ water. The absorbance at 510 nm was then measured with an UV–vis spectrophotometer and plotted against standards prepared with the same procedure starting from a commercial iron AAS standard solution.

Transmission Electron Microscopy (TEM) characterization. TEM images were collected through a Zeiss Libra 200 FE equipped with an in column pre-aligned omega filter that improves the contrast and a Schottky field emission gun at 200 kV. Samples were prepared by dropping a water solution on a holy carbon copper grid, and after blotting the excess of water, the sample were let drying at least for 24 h in air. The nanoparticle size was measured by means the ITEM TEM Imaging Platform software (Olympus). For each sample the measured NPs were around 400.

Reflected light microscopy. Experiments on cells were performed using Hela cells (ATCC CCL- 2) grown under standard conditions (5% CO_2, 37 °C) in MEM medium (Gibco) supplemented with 10% fetal bovine serum (FBS from Gibco) (complete cell culture medium, CMEM). Samples for imaging were prepared by placing glass coverslips (VWR) on the bottom of a 24 wells plate before seeding cells. Hela cells were seeded at density 30×10^4 cells per well in 0.5 mL of complete medium. After 24 h of incubation at 37 °C in 5% CO_2 the cell culture medium was replaced with freshly prepared dispersions in CMEM of SPION@ISA23-ND at a concentration of 50 μg/mL. After the required exposure times (24 h) the cells were washed once with CMEM (0.5 mL x 1) and with PBS (0.5 mL x 2), in order to remove the non-internalized NPs. Cells were fixed with 0.5 mL of formaldehyde (4%) for 15 min and then permeabilized with 0.5 mL 0.1% triton for 5 min. The cover slips were then washed three times with PBS. The lysosomes were stained with a primary mouse monoclonal antibody against the lysosomal protein Lamp-1 (lysosome-associated membrane protein 1; antibody from BD Biosciences US) (dilution in PBS 1:100), and an Alexa Fluor-488 conjugated goat anti mouse secondary antibody (Thermo Fisher Scientific) (dilution in PBS 1:200), each for 60 min. The cover slips were mounted on a glass microscopy slide with Mowiol 4–88 mounting medium (EMD Chemical, Inc., CA, USA) and analysed after 24 h of incubation at RT in dark. Analysis was performed with a confocal microscope Leica TCS SP8: in order to detect the presence of nanoparticles, the reflected light was collected by placing the emission detector in the middle of the laser (excitation) beam. The settings were as follows: reflected light: 488 nm illumination and detector: 480–505 nm; Alexa Fluor 488 excitation: 488 nm laser; Alexa Fluor 488 detector: 500–550 nm.

4.3. Syntheses

4.3.1. Synthesis of superparamagnetic iron oxide nanoparticles (SPION)

The synthesis of SPION was performed following a slightly modified literature procedure [44]. Briefly for *preparation A*, in a 50 mL three-necked round bottom flask 13.9 mmol of oleic acid (4.38 mL, d = 0.895 *g*/mL) and 2 mmol of $Fe(CO)_5$ (236 μL, d = 1.49 *g*/mL) were dissolved under inert atmosphere in 4 mL of 1-octadecene. In the second *preparation (B)* the total amount was increased and a 250 mL three-necked round-bottom flask employed, in which 60 mmol of oleic acid (19 mL, d = 0.895 *g*/mL) and 10 mmol of $Fe(CO)_5$ (1.348 mL, d = 1.49 *g*/mL) were dissolved under inert atmosphere in 40 mL of 1-octadecene. These solutions were then heated from room temperature to 320 °C at a rate of 15 °C/min and refluxed for 3 h. During this time the reddish solutions turned to black. The solutions were then cooled to 120 °C at a rate of 5 °C/min and maintained at that temperature for 2 more hours in air to allow oxidation of Fe(0). The solutions were cooled down to room temperature at a rate of 5 °C/min. The SPION were subsequently isolated by centrifugation of the reaction mixture after addition of ca 70 mL (or 500 mL in the second procedure) of acetone (4 centrifugation cycles for 5 min at 5000 round centrifugal force, rcf) followed by removal of the yellow supernatant and addition of fresh acetone. The isolated particles were then re-suspended in 15 mL (or 30 mL in the second procedure) of hexane and stored under nitrogen atmosphere at -25 °C for further uses.

4.3.2. Synthesis of nitrodopamine

Dopamine·HCl (498 mg, 2.62 mmol) and $NaNO_3$ (633 mg, 9.16 mmol) were dissolved at 0 °C in 15 mL water in a two-necked 50 mL round bottom flask under inert atmosphere. Then, 5 mL of 20% H_2SO_4 was added dropwise in the dark. The reaction mixture was left overnight at room temperature under magnetic stirring. The yellow precipitate was then filtered off, washed with ice cold water and cold methanol, and subsequently dried in vacuum, affording 338 mg of nitrodopamine.H_2SO_4 (1.14 mmol, 50.5% yield). ^1H NMR (DMSO-d_6, 300 K, 9.4 T): δ 7.45 (1H, CH), 6.60 (1H, CH), 3.05 (4H, CH_2).

4.3.3. Synthesis of ISA23-nitrodopamine conjugate (ISA23-ND)

Parent ISA23 (Mn = 29940, Mw = 44060, PD = 1.47), synthesized as described in reference [30], (335 mg, 1 mmol) was dissolved in degassed 2-(N-morpholino)ethanesulfonic acid (MES) buffer (20 mL,

0.1 M) under inert atmosphere. The pH of the solution was then carefully adjusted to 5.6 by addition of few drops of NaOH 1 M. Then, nitrodopamine (296 mg, 1 mmol) was added, and the pH adjusted to 5.6, before the addition of the cross-linker EDC (1-ethyl-3-(3-dimethylaminopropyl)carbodiimide hydrochloride, 575.1 mg, 3 mmol). The turbid yellow suspension quickly became less opaque. The reaction was left in the dark for 4 h under magnetic stirring and then filtered through a 3 kD cut-off centrifugal device to eliminate all the unreacted nitrodopamine, as well as the byproducts deriving from EDC, and further washed with water. The remaining yellow solution was lyophilized, finally affording 146.7 mg of a fluffy yellow product, ISA23-ND (42% yield). ^{1}H-NMR (D_2O, 300 K, 9.4 T): δ 8.75 (1H, NHCO), 8.66 (1H, NHCO), 8.02 (1H, CH dopamine), 6.46 (1H, CH dopamine), 5.65 (1H, NHCOC*H*NHCO of minority fraction), 5.42 (1H, NHCOC*H*NHCO of majority fraction), 3.75-2.25 (14 H CH_2 and 1H CH of 2-Me-piperazine), 1.20 (3H, CH_3).

4.3.4. One-step ligand exchange

A n-hexane suspension of SPION@OA (320 µL, 15 mg/mL Fe_3O_4, *preparation A*) was first treated with 1.5 mL EtOH to eliminate the possible excess of OA, and the NPs recovered with a magnet and redispersed in 8 mL n-hexane. To this suspension a solution of the polymer ISA23-ND (14.4 mg dissolved in 12 mL water) was added, and the pH adjusted 3–4 with the addition of 80 µL 1 M HCl. The mixture was subsequently vortexed until an emulsion was formed and then left shaking for 72 h with a vortex mixer. The organic phase became completely colorless, while the water phase passed from light yellow to brown. This last one was washed once with 10 mL hexane to remove possible OA still present. After the most of the organic phase was removed, the residues of hexane still present in the water phase were evaporated off at rotary evaporator. The water suspended SPION@ISA23-ND were then collected via centrifugation (10 min at 5000 rcf) before discarding the supernatant and re-dispersing the product in 5 mL water. This procedure was repeated twice in order to remove any remaining unbound polymer.

4.3.5. Two-step ligand exchange with TMAOH

A solution of SPION@OA in hexane (430 µL, 10 mg Fe_3O_4, *preparation B*) was dried under a gentle N_2 stream in a glass vial. Subsequently, a solution of TMAOH·5H_2O (450 mg dissolved in 2.36 mL water) was added and the vial was placed in an ultrasonic bath for few minutes in order to re-disperse the SPION. Then, the so obtained turbid suspension was diluted to 20 mL, affording a final concentration of Fe_3O_4 of 0.5 mg /mL. Ten milliliters of this solution (5 mg SPION@TMAOH) were centrifuged (5 min, 20,800 rcf), the NP pellet re-dispersed in a water solution of ISA23-ND (15 mg in 10 mL water, pH 3) and left shaking for 72 h on a vortex mixer at room temperature. Then, the SPION@ISA23-ND were recovered with a magnet and redispersed in 10 mL milliQ water. Finally, the pH was increased to 9–10 and the solution was left shaking for other 24 h. The so obtained suspension was lyophilized giving rise to a brown powder, which was promptly re-suspended in milliQ water by gently shaking.

4.3.6. Synthesis of ISA23SH-ND conjugate

$ISA23SH_{10\%}$ (Mn = 8250, Mw = 7000, PD = 1.18), prepared as previously described [67], (30 mg, 0.092 mmol) was dissolved under N_2 atmosphere in 3 mL of 0.1 M MES buffer. To this solution nitrodopamine hydrogen sulphate (25.5 mg, 0.086 mmol) was added, forming a yellow suspension. Then, EDC (47.9 mg, 0.25 mmol) was added, and the pH was adjusted to 5.4 with addition of 1 M NaOH. The reaction proceeded for 4 h at room temperature, then filtered through a 3 kD cut-off centrifugal device to eliminate unreacted nitrodopamine, EDC and byproducts, and further washed with water until the filtrate portion resulted colorless. The retained yellow fraction was then recovered and lyophilized, obtaining 15.2 mg of ISA23SH-ND copolymer.

4.3.7. Synthesis of ethylmaleimido-rhodamineB

The synthesis of 2-aminoethylmaleimide trifluoroacetate salt was carried out following a literature procedure [68]. 2-aminoethylmaleimide trifluoroacetate salt (2.4 mg, 9.3×10^{-3} mmol) was dissolved in an amber glass schlenk flask, under N_2 atmosphere, in 0.5 mL EtOH. Then, a solution of rhodamine B isothiocyanate (4.7 mg, 9.3×10^{-3} mmol) and triethylamine (1.7 µL, 1.3 eq) in 0.7 mL EtOH was added. The reaction was carried out in 12 h, at room temperature, in the dark and under magnetic stirring. The product was not isolated, and the solution used as it was for the next synthetic step.

4.3.8. Conjugation of ISA23SH-ND with rhodamineB

ISA23SH-ND (15.2 mg, 0.0436 mmol) was dissolved in 3.33 mL water in a Schlenk flask under inert atmosphere. To this solution 0.67 mL of ethanol solution of ethylmaleimido-rhodamineB (2.8 mg, 1 eq. with respect to –SH groups) was added. The reaction was left at room temperature in the dark for 72 h, then filtered through a 3 kD cut-off centrifugal device to eliminate unreacted rhodamine and further washed with water until the filtrate portion resulted colorless. The solution was then lyophilized, recovering a purple polymer that was then dissolved in 2 mL milliQ water. The rhodamineB concentration in this solution was determined spectrophotometrically, using its known ε_{560} = 86.000, and was found to be 0.2 mM.

4.3.9. Two-step ligand exchange with ISA23SH-ND-RhodamineB

A hexane SPION@OA clear suspenion (430 µL, 10 mg Fe_3O_4) was dried under gentle N_2 stream in a glass vial. Then, a solution of TMAOH·5H_2O (450 mg dissolved in 2.36 mL water) was added and the vial was placed in an ultrasonic bath in order to redisperse the SPIONs. The resultant suspension was diluted to 20 mL with milliQ water, affording a final 0.5 mg /mL Fe_3O_4 concentration. An aliquot of this suspension (6 mL, 3 mg Fe_3O_4@TMAOH) was centrifuged (7.5 min, 20,800 rcf) to eliminate the most excess TMAOH, then the pellet was redispersed in 6 mL of ISA23SH-ND-RhodamineB solution (3 mg, pH 3) and left shaking for 72 h on a vortex mixer. The excess polymer was removed by centrifugation (5 min x 20.000 rcf). The retrieved NPs were washed twice with milliQ water and finally recovered by centrifugation (10 min x 10.000 rcf).

4.3.10. Determination of bovine serum albumin adsorbed on SPION@ISA23-ND and SPION@TMAOH

The NPs (0.3 mL containing 0.35 mg/mL of SPION@TMAOH or SPION@ISA23-ND) were added to 1 mL of phosphate buffer solution (10^{-3} M, total ionic strength 0.05 adjusted by addition of KNO_3) of bovine serum albumin (BSA, 0.1 mg/mL). The suspensions were incubated for 90 min at room temperature on a vortex mixer. The magnetic nanocomposites were then separated in a pellet by centrifugation for 15 min at 20,100 *g*, before determining the relative concentration of BSA in the supernatant by UV–vis spectroscopy comparing the absorbance (λ_{max} = 278 nm) with the one of the native BSA solution.

Acknowledgements

Klaas Sjollema (UMCG Imaging facility, Groningen) is kindly acknowledged for assistance with reflected light microscopy. DM thanks Università degli Studi di Milano for supporting the research (Piano di sviluppo dell'Ateneo -2017 Linea 2 Azione B). The use of equipment purchased through the Regione Lombardia – Fondazione Cariplo joint SmartMatLab Project (2013-1766) is gratefully acknowledged.

Appendix A. Supplementary data

Supplementary material related to this article can be found, in the online version, at doi:https://doi.org/10.1016/j.colsurfb.2018.11.007.

References

[1] L.H. Reddy, J.L. Arias, J. Nicolas, P. Couvreur, Magnetic nanoparticles: design and characterization, toxicity and biocompatibility, pharmaceutical and biomedical applications, Chem. Rev. 112 (2012) 5818–5878.

[2] Y.X.J. Wang, S.M. Hussain, G.P. Krestin, Superparamagnetic iron oxide contrast agents: physicochemical characteristics and applications in MR imaging, Eur. Radiol. 11 (2001) 2319–2331.

[3] B. Gleich, J. Weizenecker, Tomographic imaging using the nonlinear response of magnetic particles, Nature 435 (2005) 1214–1217.

[4] N. Panagiotopoulos, F. Vogt, J. Barkhausen, T.M. Buzug, R.L. Duschka, K. Lüdtke-Buzug, M. Ahlborg, G. Bringout, C. Debbeler, M. Gräser, C. Kaethner, J. Stelzner, H. Medimagh, J. Haegele, Magnetic particle imaging: current developments and future directions, Int. J. Nanomed. (2015) 3097.

[5] S. Laurent, S. Dutz, U.O. Häfeli, M. Mahmoudi, Magnetic fluid hyperthermia: focus on superparamagnetic iron oxide nanoparticles, Adv. Colloid Interface Sci. 166 (2011) 8–23.

[6] Y. Piñeiro, Z. Vargas, J. Rivas, M.A. Lõpez-Quintela, Iron oxide based nanoparticles for magnetic hyperthermia strategies in biological applications, Eur. J. Inorg. Chem. 2015 (2015) 4495–4509.

[7] S. Sun, H. Zeng, Size-controlled synthesis of magnetite nanoparticles, J. Am. Chem. Soc. 124 (2002) 8204–8205.

[8] J. Park, K. An, Y. Hwang, J.-G. Park, H.-J. Noh, J.-Y. Kim, J.-H. Park, N.-M. Hwang, T. Hyeon, Ultra-large-scale syntheses of monodisperse nanocrystals, Nat. Mater. 3 (2004) 891–895.

[9] D. Ling, N. Lee, T. Hyeon, Chemical synthesis and assembly of uniformly sized iron oxide nanoparticles for medical applications, Acc. Chem. Res. 48 (2015) 1276–1285.

[10] W. Wu, Q. He, C. Jiang, Magnetic iron oxide nanoparticles: synthesis and surface functionalization strategies, Nanoscale Res. Lett. 3 (2008) 397–415.

[11] H. Maeda, J. Wu, T. Sawa, Y. Matsumura, K. Hori, Tumor vascular permeability and the EPR effect in macromolecular therapeutics: a review, J. Control. Release 65 (2000) 271–284.

[12] T.D. Schladt, K. Schneider, H. Schild, W. Tremel, Synthesis and bio-functionalization of magnetic nanoparticles for medical diagnosis and treatment, Dalton Trans. 40 (2011) 6315–6343.

[13] S. Mondini, M. Leonzino, C. Drago, A.M. Ferretti, S. Usseglio, D. Maggioni, P. Tornese, B. Chini, A. Ponti, Zwitterion-coated iron oxide nanoparticles: surface chemistry and intracellular uptake by hepatocarcinoma (HepG2) cells, Langmuir 31 (2015) 7381–7390.

[14] A. Prakash, H. Zhu, C.J. Jones, D.N. Benoit, A.Z. Ellsworth, E.L. Bryant, V.L. Colvin, Bilayers as phase transfer agents for nanocrystals prepared in nonpolar solvents, ACS Nano 3 (2009) 2139–2146.

[15] M. Muthiah, I.-K. Park, C.-S. Cho, Surface modification of iron oxide nanoparticles by biocompatible polymers for tissue imaging and targeting, Biotechnol. Adv. 31 (2013) 1224–1236.

[16] J.W.M. Bulte, Y. Hoekstra, R.L. Kamman, R.L. Magin, A.G. Webb, R.W. Briggs, K. Gwan Go, C.E. Hulstaert, S. Miltenyi, T. Hauw The, L. De Leij, Specific MR imaging of human lymphocytes by monoclonal antibody-guided dextran-magnetite particles, Magn. Reson. Med. 25 (1992) 148–157.

[17] K. Kang, J. Choi, J.H. Nam, S.C. Lee, K.J. Kim, S.-W. Lee, J.H. Chang, Preparation and characterization of chemically functionalized silica-coated magnetic\rnano-particles as a DNA separator, J. Phys. Chem. B 113 (2009) 536–543.

[18] J. Lee, Y. Lee, J.K. Youn, H. Bin Na, T. Yu, H. Kim, S.-M. Lee, Y.-M. Koo, J.H. Kwak, H.G. Park, H.N. Chang, M. Hwang, J.-G. Park, J. Kim, T. Hyeon, Simple synthesis of functionalized superparamagnetic magnetite/silica core/shell nanoparticles and their application as magnetically separable high-performance biocatalysts, Small 4 (2008) 143–152.

[19] A. Narita, K. Naka, Y. Chujo, Facile control of silica shell layer thickness on hydrophilic iron oxide nanoparticles via reverse micelle method, Colloids Surf. A Physicochem. Eng. Asp. 336 (2009) 46–56.

[20] M. Zhang, B.L. Cushing, C.J. O'Connor, Synthesis and characterization of monodisperse ultra-thin silica-coated magnetic nanoparticles, Nanotechnology 19 (2008) 85601.

[21] A.K. Gupta, S. Wells, Surface-modified superparamagnetic nanoparticles for drug delivery: preparation, characterization, and cytotoxicity studies, IEEE Trans. Nanobiosci. 3 (2004) 66–73.

[22] J.Y. Park, P. Daksha, G.H. Lee, S. Woo, Y. Chang, Highly water-dispersible PEG surface modified ultra small superparamagnetic iron oxide nanoparticles useful for target-specific biomedical applications, Nanotechnology 19 (2008) 365603.

[23] J. Xie, C. Xu, N. Kohler, Y. Hou, S. Sun, Controlled PEGylation of monodisperse Fe3O4 nanoparticles for reduced non-specific uptake by macrophage cells, Adv. Mater. 19 (2007) 3163–3166.

[24] D. Müller-Schulte, Magnetic Polymer Particle on the Basis of Poly(vinyl Alcohol), Process for Its Preparation and Application Thereof, PCT/EP/96 02398, (1996).

[25] S.J. Yoon, S.Y. Jun, A.S. Kwon, S.H. Kang, Y.Y. Jeong, I.K. Park, C.S. Cho, Y.K. Kim, W.J. Kim, R. Namgung, MRI Contrast Agent Coated With Carboxylated Mannan and Method for Producing the Same, Patent number: 8961935 Intron Biotechnology, Inc.), 2015.

[26] Y. Ying, N. Erathodiyil, A.W.H. Lin, S.T. Selvin, Polymer Coated Magnetic Particles, Jackie WO2011053252A1, Agency For Science, Technology And Research, 2011.

[27] E.A. Millan, P.F. Palacio, R.G. Ibarz, B.E. Natividad, Systems Containing Magnetic Nanoparticles and Polymers, Such As Nanocomposites and Ferrofluids, and Applications Thereof. WO2008034675A1 (Consejo Superior De Investigaciones Científicas), (2008).

[28] G. Baldi, D. Bonacchi, F. Innocenti, G. Lorenzi, M. Bitossi, P. Ferruti, E. Ranucci, A. Ricci, M. Comes Franchini, Magnetic Nanoparticles for the Application in Hyperthermia, Preparation Thereof and Use in Constructs Having a Pharmacological Application, Publication number: 20100015060 (COLOROBBIA ITALIA S.P.A. (2010).

[29] S. Zapotoczny, G. Kania, A. Szpak, M. Nowakowska, Superparamagnetic Iron Oxide Nanoparticles With Ultra-thin Polymer Layers, the Method of Their Preparation and Application (Uniwersytet Jagiellonski) WO2014081322A1, (2014).

[30] S. Richardson, P. Ferruti, R. Duncan, Poly(amidoamine)s as potential endosomolytic polymers: evaluation in vitro and body distribution in normal and tumour-bearing animals, J. Drug Target. 6 (1999) 391–404.

[31] P. Ferruti, E. Ranucci, L. Sartore, F. Bignotti, M.A. Marchisio, P. Bianciardi, F.M. Veronese, Recent results on functional polymers and macromonomers of interest as biomaterials or for biomaterial modification, Biomaterials 15 (1994) 1235–1241.

[32] P. Ferruti, E. Ranucci, F. Bignotti, L. Sartore, P. Bianciardi, M.A. Marchisio, Degradation behaviour of ionic stepwise polyaddition polymers of medical interest, J. Biomat. Sci. Polym. Ed. 6 (1994) 833–844.

[33] D. Maggioni, M. Galli, L. D'Alfonso, D. Inverso, M.V. Dozzi, L. Sironi, M. Iannacone, M. Collini, P. Ferruti, E. Ranucci, A luminescent poly (amidoamine)–iridium complex as a new singlet-oxygen sensitizer for photodynamic therapy, Inorg. Chem. 54 (2015) 544–553.

[34] D. Maggioni, F. Fenili, L. D'Alfonso, D. Donghi, M. Panigati, I. Zanoni, R. Marzi, A. Manfredi, P. Ferruti, G. D'Alfonso, Luminescent rhenium and ruthenium complexes of an amphoteric poly (amidoamine) functionalized with 1, 10-phenanthroline, Inorg. Chem. 51 (2012) 12776–12788.

[35] P. Ferruti, Poly(amidoamine)s: past, present, and perspectives, J. Polym. Sci. Part A Polym. Chem. 51 (2013) 2319–2353.

[36] E. Ranucci, P. Ferruti, E. Lattanzio, A. Manfredi, M. Rossi, P.R. Mussini, F. Chiellini, C. Bartoli, Acid-base properties of poly(amidoamine)s, J. Polym. Sci. Part A Polym. Chem. 47 (2009) 6977–6991.

[37] J.B. Neilands, Siderophores: structure and function of microbial iron transport compounds, J. Biol. Chem. 270 (1995) 26723–26726.

[38] H. Lee, S.M. Dellatore, W.M. Miller, P.B. Messersmith, Mussel-inspired surface chemistry for multifunctional coatings, Science (80-.) 318 (2007) 426–430.

[39] S. Mondini, C. Drago, A.M. Ferretti, A. Puglisi, A. Ponti, Colloidal stability of iron oxide nanocrystals coated with a PEG-based tetra-catechol surfactant, Nanotechnology 24 (2013) 105702.

[40] T. Orlando, A. Paolini, F. Pineider, E. Clementi, F. Pasi, Y. Guari, J. Larionova, L. Sacchi, R. Nano, M. Corti, A. Lascialfari, NMR as evaluation strategy for cellular uptake of nanoparticles, Nano Lett. 14 (2014) 3959–3965.

[41] V.M. Nurchi, T. Pivetta, J.I. Lachowicz, G. Crisponi, Effect of substituents on complex stability aimed at designing new iron(III) and aluminum(III) chelators, J. Inorg. Biochem. 103 (2009) 227–236.

[42] A. Manfredi, F. Carosio, P. Ferruti, E. Ranucci, J. Alongi, Linear polyamidoamines as novel biocompatible phosphorus-free surface-confined intumescent flame retardants for cotton fabrics, Polym. Degrad. Stab. 151 (2018) 52–64.

[43] D.A. Tomalia, H. Baker, J. Dewald, M. Hall, G. Kallos, S. Martin, J. Roeck, J. Ryder, P. Smith, A new class of polymers: starburst-dendritic macromolecules, Polym. J. 17 (1985) 117–132.

[44] P. Calcagnile, D. Fragouli, I.S. Bayer, G.C. Anyfantis, L. Martiradonna, P.D. Cozzoli, R. Cingolani, A. Athanassiou, Magnetically driven floating foams for the removal of oil contaminants from water, ACS Nano 6 (2012) 5413–5419.

[45] H. Bin Na, G. Palui, J.T. Rosenberg, X. Ji, S.C. Grant, H. Mattoussi, Multidentate catechol-based polyethylene glycol oligomers provide enhanced stability and biocompatibility to iron oxide nanoparticles, ACS Nano 6 (2012) 389–399.

[46] K.H. Bae, M. Park, M.J. Do, N. Lee, J.H. Ryu, G.W. Kim, C. Kim, T.G. Park, T. Hyeon, Chitosan oligosaccharide-stabilized ferrimagnetic iron oxide nanocubes for magnetically modulated cancer hyperthermia, ACS Nano 6 (2012) 5266–5273.

[47] C. Xu, K. Xu, H. Gu, R. Zheng, H. Liu, X. Zhang, Z. Guo, B. Xu, Dopamine as A robust anchor to immobilize functional molecules on the iron oxide shell of magnetic nanoparticles, J. Am. Chem. Soc. 126 (2004) 9938–9939.

[48] D. Maggioni, P. Arosio, F. Orsini, A.M. Ferretti, T. Orlando, A. Manfredi, E. Ranucci, P. Ferruti, G. D'Alfonso, A. Lascialfari, Superparamagnetic iron oxide nanoparticles stabilized by a poly (amidoamine)-rhenium complex as potential theranostic probe, Dalton Trans. 43 (2014) 1172–1183.

[49] E.J. Guggenheima, I. Lynch, J.Z. Rappoport, Imaging in focus: reflected light imaging: techniques and applications, Int. J. Biochem. Cell Biol. 83 (2017) 65–70.

[50] E.J. Guggenheim, A. Khan, J. Pike, L. Chang, I. Lynch, J.Z. Rappoport, Comparison of confocal and superresolution reflectance imaging of metal oxide nanoparticles, PLoS One 11 (2016) e0159980.

[51] J. Mazzolini, R.J.M. Weber, H.-S. Chen, A. Khan, E. Guggenheim, R.K. Shaw, J.K. Chipman, M.R. Viant, J.Z. Rappoport, Protein corona modulates uptake and toxicity of nanoceria via clathrin-mediated endocytosis, Biol. Bull. 231 (2016) 40–60.

[52] C.S. Kim, X. Li, Y. Jiang, B. Yan, G.Y. Tonga, M. Ray, D.J. Solfiell, V.M. Rotello, Cellular imaging of endosome entrapped small gold nanoparticles, MethodsX 2 (2015) 306–315.

[53] A. Salvati, C. Åberg, T. dos Santos, J. Varela, P. Pinto, I. Lynch, K.A. Dawson, Experimental and theoretical comparison of intracellular import of polymeric nanoparticles and small molecules: toward models of uptake kinetics, Nanomed. Nanotechnol. Biol. Med. 7 (2011) 818–826.

[54] V. Salgueiriño-Maceira, L.M. Liz-Marzán, M. Farle, Water-based ferrofluids from Fe x Pt 1- x nanoparticles synthesized in organic media, Langmuir 20 (2004) 6946–6950.

[55] P. Guardia, N. Pérez, A. Labarta, X. Batlle, Controlled synthesis of iron oxide

nanoparticles over a wide size range, Langmuir 26 (2010) 5843–5847.
[56] L.E. Euliss, S.G. Grancharov, S. O'Brien, T.J. Deming, G.D. Stucky, C.B. Murray, G.A. Held, Cooperative assembly of magnetic nanoparticles and block copolypeptides in aqueous media, Nano Lett. 3 (2003) 1489–1493.
[57] Â.L. Andrade, J.D. Fabris, J.D. Ardisson, M.A. Valente, J.M.F. Ferreira, Effect of tetramethylammonium hydroxide on nucleation, surface modification and growth of magnetic nanoparticles, J. Nanomater. 2012 (2012) 1–10.
[58] M. Galli, A. Guerrini, S. Cauteruccio, P. Thakare, D. Dova, F. Orsini, P. Arosio, C. Carrara, C. Sangregorio, A. Lascialfari, D. Maggioni, E. Licandro, Superparamagnetic iron oxide nanoparticles functionalized by peptide nucleic acids, RSC Adv. 7 (2017) 15500–15512.
[59] T. Blunk, D.F. Hochstrasser, J.C. Sanchez, B.W. Müller, R.H. Müller, Electrophoresis 14 (1993) 1382–1387.
[60] J.S. Suk, Q. Xu, N. Kim, J. Hanes, L.M. Ensign, PEGylation as a strategy for improving nanoparticle-based drug and gene delivery, Adv. Drug. Deliv. Rev. 99 (2016) 28–51.
[61] S. Kumar, I. Yadav, V.K. Aswal, J. Kohlbrecher, Structure and interaction of nanoparticle-protein complexes, Langmuir 34 (2018) 5679–5695.
[62] R. Cavalli, C. Bocca, A. Miglietta, O. Caputo, M.R. Gasco, Albumin adsorption on stealth and non-stealth solid lipid nanoparticles, S.T.P. Pharma Sci. 9 (1999) 183–189.
[63] J. Lee, P.A. Martic, J.S. Tan, Protein adsorption on pluronic copolymer-coated polystyrene particles, J. Colloid Interface Sci. 131 (1989) 252–266.
[64] R. Serrano García, S. Stafford, Y.K. Gun'ko, Recent progress in synthesis and functionalization of multimodal fluorescent-magnetic nanoparticles for biological applications, Appl. Sci. 8 (2018) 172–195.
[65] D. Kruk, A. Korpała, S.M. Taheri, A. Kozłowski, S. Förster, E.A. Rössler, 1 H relaxation enhancement induced by nanoparticles in solutions: Influence of magnetic properties and diffusion, J. Chem. Phys. 140 (2014) 174504.
[66] H. Amiri, R. Bustamante, A. Millán, N.J.O. Silva, R. Piñol, L. Gabilondo, F. Palacio, P. Arosio, M. Corti, A. Lascialfari, Magnetic and relaxation properties of multifunctional polymer-based nanostructured bioferrofluids as MRI contrast agents, Magn. Reson. Med. 66 (2011) 1715–1721.
[67] D. Donghi, D. Maggioni, G. D'Alfonso, F. Amigoni, E. Ranucci, P. Ferruti, A. Manfredi, F. Fenili, A. Bisazza, R. Cavalli, Tricarbonyl-rhenium complexes of a thiol-functionalized amphoteric poly(amidoamine), Biomacromolecules 10 (2009) 3273–3282.
[68] M. Richter, A. Chakrabarti, I.R. Ruttekolk, B. Wiesner, M. Beyermann, R. Brock, J. Rademann, Multivalent design of apoptosis-inducing Bid-BH3 peptide-oligosaccharides boosts the intracellular activity at identical overall peptide concentrations, Chem. – A Eur. J. 18 (2012) 16708–16715.